TEXTURAL FRACTOGRAPHY

Hynek Lauschmann, Ondřej Ráček, Michal Tůma, Ivan Nedbal

Czech Technical University, Faculty of Nuclear Sciences & Physical Engineering, Dept. of Materials
Trojanova 13, 12000 Praha 2, Czech Republic
lausch@kmat.fjfi.cvut.cz

Abstract. The reconstitution of the history of a fatigue process is based on the knowledge of any correspondences between the morphology of crack surface and the velocity of crack growth (crack growth rate - CGR). The textural fractography is oriented to mezoscopic SEM magnifications (30÷500x). Images contain a complicated texture without distict borders. The aim is to find any characteristics of this texture which correlate with CGR. Pre-processing of images is necessary to obtain a homogeneous texture. Three methods of textural analysis have been developed and realized as computational programs in MATLAB: method based on the spectral structure of the image, method based on a Gibbs random field (GRF) model, and method based on the idealisation of light objects into a fibre process. To extract and analyze the fibre process, special methods - tracing fibres and a database oriented analysis of a fibre process, have been developed.

Keywords: database, fatigue, fibre process, Fourier transform, fractography, Gibbs random field, regression, texture.

1. INTRODUCTION

The main task of the quantitative microfractography of fatigue failures is the reconstitution of the history of a fatigue crack growth process. Specimens of the material are loaded in the laboratory under service conditions and the crack growth process is recorded. Fracture surfaces are documented by SEM and images are studied to relate some information present in the morphology of the crack surface to the macroscopic crack velocity (crack growth rate - CGR). So a basis is obtained on which an unknown CGR can be estimated from fracture surfaces of real parts. Finally, the crack growth process is reconstituted using integration of CGR along the crack growth direction.

The traditional method is based on striations, fine equidistant grooves in the fracture surface [3]. They belong to fractographic features - strictly defined measurable objects in the morphology of the fracture surface. The method cannot be used when striations are not visible, typically due to corrosion.

As an alternative, the textural method has been developed in our department since about 1990. Structures in images of fracture surfaces are studied as image textures. The texture is a random structure of similar elements with some kind of ordering. The main problem in fractography consists in a continuous brightness scale and an absence of distinct borders of textural elements.

Suitable for the application of the textural method is especially the mezoscopic dimensional area with SEM magnifications between macro- and microfractography (about 30 ÷ 500 x). These magnifications were not used very much in the past for the absence of measurable objects in images. The magnification to be used is limited by several conditions related to individual images, to the whole set of images and to the image discretization. Images must be pre-processed to obtain a homogeneous texture which is convenient for the analysis.

Within the textural method, fractographic information is extracted in the form of integral parameters of the whole image. Two general approaches to the analysis have been studied:
1. computing statistical or model parameters directly from gray-scale images without any respect to textural elements.
2. extraction of textural elements followed by the application of binary random field models.

For developing algorithms and computationl programs, MATLAB with Image Processing Toolbox was used.

2. EXPERIMENT

Methods developed will be shown in an application to fatigue fracture surfaces of four laboratory specimens (C16÷19) of the stainless steel AISI 304L used in nuclear power plants [9]. CT (compact tension) specimens (Fig.1) were loaded by constant cycle with parameters $\Delta F = 3400$ N, $R = 0.3$, $f = 1$ Hz in water at 20°C.

Fatigue crack surfaces were documented using SEM with magnification 200x. The sequence of images was located in the middle of the crack surface (Fig.1) and the images were distanced by 0.4 mm. The direction of the crack growth in images is bottom-up. The real area of one image is about 0.6 x 0.45 mm. Digital representation in 1200 x 1600 pixels and 256 brightness values was used. The total number of images was 165. An example of a typical texture is shown in Fig.2.

From frequently repeated records of the crack length, the estimates of CGR were computed. The course of the CGR related to the crack length was estimated and every image was assessed a value of the CGR pertinent to its middle.
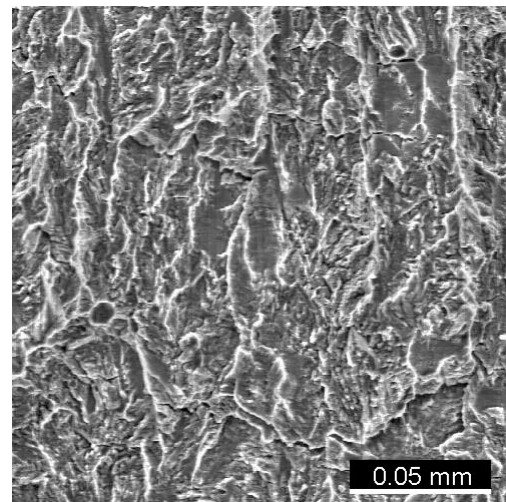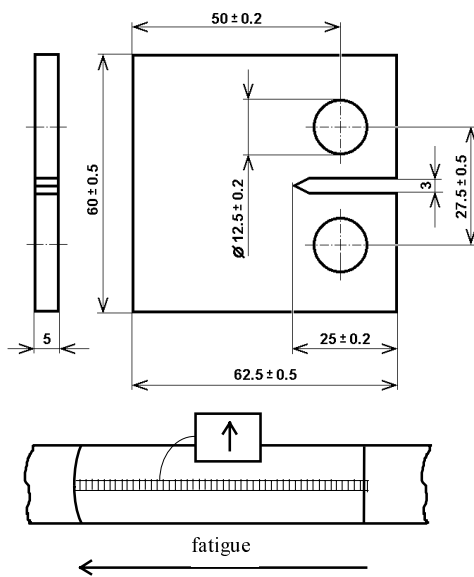

Fig. 1: Specimen for fatigue tests and loca-
ting of images in fatigue crack surface.

Fig. 2: An example of a typical texture in an ima-
ge of crack surface (detail 500x500 pixels).

3. GENERAL COMMENTS

SETTING SEM MAGNIFICATION. An appropriate magnification must be optimized with respect to several requirements [7]:

Within one image:
- the number of textural elements is representative enough to characterize the texture objectively,
- the texture is approximately homogeneous (the change with increasing CGR is negligible),
- the change of CGR within one image is negligible (it can be characterized by a constant).

Within the set of images:
- the general character of all textures is the same (the same type of analysis can be applied),
- some feature of the texture is significantly dependent on CGR.

Within the given image discretization:
- textural elements that are to be the source of information are well represented.

In practical cases, these requirements are counteracting and a compromise must be sought.

PRE-PROCESSING OF IMAGES is necessary in order to remove significant fluctuations of mean brightness and contrast. A suitable method - normalization [6] - was proposed by generalization from one-dimensional stochastic processes. The brightness is transformed by a moving algorithm to mean value 128 and standard deviation 50 (for the 8-bit range). In contrast to the generally used equalization, the shape of textural elements is conserved. The size of the mask is a very important parameter fundamentally affecting the results.

THE MULTILINEAR MODEL. The experience showed that a single image characteristic of any type is not robust enough to characterize the relation between CGR and the crack morphology. Although the dependence can be very tight within a set of images from one crack surface, on another crack surfaces (from different testing specimens) the same parameter can depend on CGR in a different way. Therefore, we estimate a set of image characteristics of the given type (for instance spectral) for every image, and this whole set is related to the value of CGR (due to general qualities of crack velocity, its logarithm $\log_{10} v$ must be considered).

The most simple model [8] expressing the CGR as a function of a set of image parameters $f_1, f_2, ..., f_k$, is a multilinear function resulting into a regression equation (1). The values of parameters c_u can be estimated using the least squares method. The input information is composed of the set of images with assigned values of the CGR. From every image, a set of image characteristics f_u is computed, completed with constant 1 and arranged into one row of matrix F (2). Then the system of equations can be written in the form (3) where L is a column vector of logarithms of CGR assigned to single images and C is a column vector of estimated parameters c_u in the sequence given by ordering values f_u into rows of matrix F.

$$\overline{\log v} = \sum_{u=1}^{k} c_u f_u + c_{k+1} \qquad (1) \qquad\qquad t_u = \frac{c_u}{s_u} \qquad (4)$$

$$F = \begin{bmatrix} f_1^1 & f_2^1 & \cdots & f_k^1 & 1 \\ \vdots & \vdots & \vdots & \vdots & \vdots \\ f_1^q & f_2^q & \cdots & f_k^q & 1 \end{bmatrix} \quad (2) \qquad s_u = \sqrt{\frac{\sum\left(\log v - \overline{\log v}\right)^2}{q-k-2}\left(\left(F'F\right)^{-1}\right)_{u,u}} \quad (5)$$

$$L = FC \qquad (3) \qquad\qquad \left|t_u\right| < t_{1-\alpha/2}\left(q-k-2\right) \qquad (6)$$

Not all characteristics f_u predicate the CGR. An instrument for testing the significance is the test of the zero value of the estimated coefficients c_u, $u=1,..., k+1$. We test the hypothesis H_0: $c_u = 0$ against the alternative H_1: $c_u \neq 0$. The test criterion is a Student's t-distributed statistic (4). If the absolute value of t_u is lower than the critical value at the selected level of significance α and q-k-2 degrees of freedom (6), the hypothesis H_0 cannot be rejected and the parametr f_u should be excluded.

A handicap originates from the multiparametric character of the method. The model counterbalances many increments from different sources of information. Therefore, a fractographic interpretation of the variety of textural elements is hardly possible.

4. METHODS

4.1 SPECTRAL ANALYSIS

The 2D Fourier transformation [1] is a decomposition of the image matrix X of the size m x n into a linear combination of basic vectors $B^{r,s}$

$$X = \sum_{r=0}^{m-1}\sum_{s=0}^{n-1} y_{r,s} B^{r,s}, \quad \text{where} \quad y_{r,s} = X * B^{r,s} = \sum_{k=1}^{m}\sum_{l=1}^{n} x_{k,l} b_{k,l}^{r,s}. \qquad (7)$$

A basic vector is a matrix of the same dimensions m x n which represents a harmonic wave with frequency r in the column direction and s in the row direction, expressed by the number of periods within the dimensions of the image. The set of coefficients $y_{r,s}$ creates a complex matrix $\boldsymbol{Y}$ of the same size as the image. The presence of single frequencies without respect to wave phases is expressed by the set of amplitudes called spectrum, $A=|\boldsymbol{Y}|$.

For the fractographic interpretation, suitable characteristics are not frequencies but distances and directions ($\theta = 0$ matches the direction bottom-up in the image) [8]. That is why we interpret the spectrum in variables [period, direction] = $[p, \theta]$. Basic vector $\boldsymbol{B}^{r,s}$ represents a harmonic wave with period (wave length) $p_{r,s}$ and normal direction (direction of the wave vector) $\theta_{r,s}$

$$p_{r,s} = \left(\frac{r^2}{m^2} + \frac{s^2}{n^2} \right)^{-1/2} \quad , \qquad \theta_{r,s} = -arctg\left(\frac{ms}{nr} \right) . \tag{8}$$

To reduce the number of output spectral characteristics, a reasonable sorting of both parameters can be introduced. Single segments of the spectrum defined by the Cartesian product of intervals of periods and directions, $[p,\theta] \in (p_i, p_{i+1})$ x (θ_j, θ_{j+1}), can be characterized by the mean spectrum

$$f_{i,j} = \sum_{r,s} a_{r,s}\delta_{r,s} \bigg/ \sum_{r,s} \delta_{r,s} , \quad \text{where } \delta_{r,s} = \Big\langle \begin{array}{l} 1 \text{ if } p_{r,s} \in \langle p_i, p_{i+1}) , \ \theta_{r,s} \in \langle \theta_j, \theta_{j+1}) , \\ 0 \text{ otherwise} . \end{array} \tag{9}$$

APPLICATION [8]. In the case mentioned above, the sorting of periods was defined in real distances by interval borders $p = \{1, 2, 3, 4, 5, 6, 8, 10, 12, 14, 16, 20, 24, 30\}$ µm. Sorting of directions was limited to 3 classes: directions close to the direction of crack growth $\theta \in(-15\div15°)$, directions close to crack front $\theta \in(-90\div-75°) \cup (75\div90°)$ and all other directions. All combinations created 45 segments. Within the application of multilinear regression (1), 19 segments of spectrum have been found to be significant at the level of significance $\alpha = 0.05$.
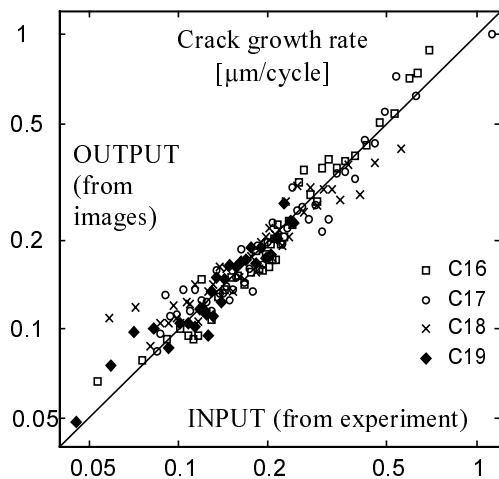

Fig. 3: Comparison of crack rates taken for input and given back from spectrum of images of crack surfaces. Ideal agreement: $y = x$.
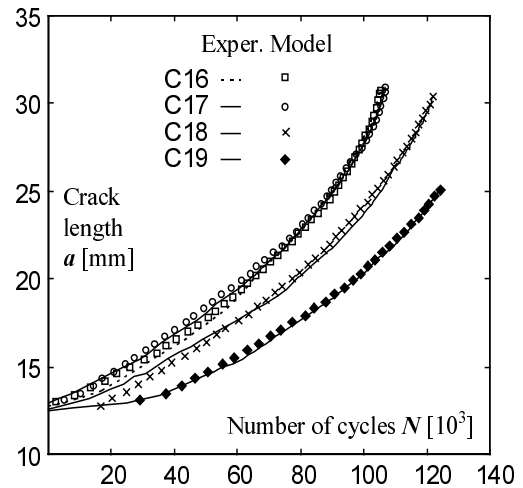
Fig. 4: Crack growth in single specimens and reversal reconstitution (from the end to the origin) using crack rates estimated from images.

A comparison of experimental CGR taken for input and CGR values given back from the spectral characteristics of images is shown in Fig.3. The relations of the crack length vs. the number of loading cycles are demonstrated in Fig.4. One point represents one image.

4.2 GIBBS RANDOM FIELDS

A simple GRF model [4,11] of a texture reflects gray levels $u(r,c)$ in single pixels, and interactions - differences $d = u_1-u_2$ between gray levels of two pixels. All pairs of pixels with the same distance vector $[i, j] = [r_1-r_2, c_1-c_2]$ create a clique. A list of cliques that are taken into account is called search window W. The distance vector $[0,0]$ represents gray levels in single pixels. At random textures, the significance of interactions decreases with the increasing distance of both pixels creating the pair.

The main sample characteristic of an image x is a gray level co-occurrence histogram $h(x)$. $h_{i,j,d}$ is the number of interactions d in clique $[i, j]$. Probability of interactions is $p_{i,j,d} = h_{i,j,d} / [(m-|i|)(n-|j|)]$, where m,n are dimensions of the image.

The main GRF characteristic is potential $V = \{V_{i,j,d}\}$. Within Gibbs probability distribution of a random field with a potential V, the probability of image x is proportional to $\exp(-V * h(x))$, where $*$ denotes a scalar product of arrays V and $h(x)$ reshaped into vectors.

For a given image x_o, potential V can be estimated in two steps: The first approximation of the potential based on Taylor expansion of the likelihood function is refined by means of stochastic relaxation. Within it, difference between the training sample x_o and current sample $x^{(t)}$ is measured by chi-square distance

$$\Delta\left(x_o, x^{(t)}\right) = \sum_{[i,j]\in W} \sum_{d \in D} \left(p_{i,j,d}(x_o) - p_{i,j,d}(x^{(t)})\right)^2 . \quad (10)$$

In the course of relaxation, the difference Δ decreases to a constant and its fluctuations to zero.

A measure of the significance of cliques $[i,j]$ are their relative energies

$$f_{i,j} = \sum_{d \in D} V_{i,j,d} \ p_{i,j,d}(x_o), \ [i,j] \in W, \quad (11)$$

from which only that for small distance components i,j are significant. The set of significant relative energies can be used for characteristics of the images to be applied in the multilinear regression (1).

APPLICATION [11]. 31 energies $f_{i,j}$ were chosen that were significant in all images. From them, 25 have been found to be significant in the multilinear regression at the level of significance $\alpha = 0.05$. The result is plotted in Fig.5. One point represents one image. The relation of the crack length vs. the number of cycles is not visibly different from that in Fig.4.

Fig. 5: Comparison of crack rates taken for input and given back from the GRF model of image texture. Ideal agreement: $y = x$.

4.3 FIBRE PROCESS

In many cases, the most remarkable elements of textures are light fibres with a different thickness and shape. They reflect sharp ridges and edges in the fracture surface. This structure can be abstracted into a fibre process [5], whose qualities are studied to find any sensitivity to the velocity of the crack growth. The length of continuous fibres is an important property. The requirement of analyzing the continuity of fibres in knots made it necessary to create a database of the structure of the fibre process. Consequently it was found that such a database can be used to estimate many important characteristics of the process.
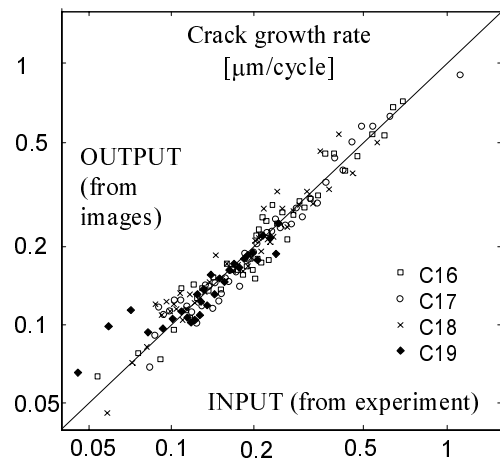
First we will show how fibre processes may be extracted from fractographic images, and then the creation and utilizing of the database will be described.

EXTRACTION OF FIBRES. Images were normalized to receive a homogeneous texture (Fig.6a), [6]. The binarization by threshold met troubles because objects received did not respond with qualities of fibres at any value of threshold. A procedure, aimed at light fibre objects on purpose, was proposed in following steps:

1. Marr & Hildreth edge detection [2,13] modified on fibres. The basis is convolution mask

$$U_{2,5} = \begin{bmatrix} -1 & -3 & 9 & -3 & -1 \\ -1 & -3 & 9 & -3 & -1 \end{bmatrix}, \quad (12)$$

which enhances a vertical light fibre of the width 1 or 2 pixels. By rescaling the mask into $U_{r,s}$ the effect can be optimized to a fibre width about $s/3$ and a length of a direct element r. In our case, $U_{5,12}$ was rotated by $0, \pi/8, \ldots , 7\pi/8$ and the maximum of all applications was taken for the result (Fig.6b).

2. From the starting points - the lightest pixels of the image, fibres are traced towards both sides using a set of directional modifications of the mask [10,13]

$$V_0 = \begin{bmatrix} 0 & 0 & 0 & 0 & 0 & 0 & 0 \\ 0 & 0 & 0 & 0 & 0 & 0 & 0 \\ 0 & 0 & 0.5 & 0.5 & 1 & 1 & 1 \\ \{1\} & 1 & 1 & 1 & 1 & 1 & 1 \\ 0 & 0 & 0.5 & 0.5 & 1 & 1 & 1 \\ 0 & 0 & 0 & 0 & 0 & 0 & 0 \\ 0 & 0 & 0 & 0 & 0 & 0 & 0 \end{bmatrix}, \quad (13)$$

where {1} denotes the position of the last recognized crack pixel. The direction related to the maximal result of convolutions is accepted for the step of tracing the crack.
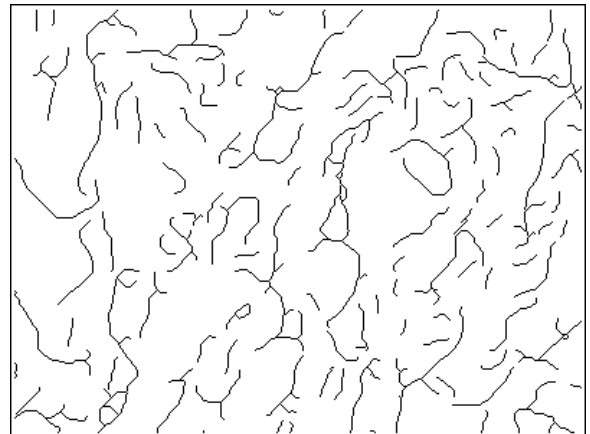
To avoid a double tracing or reversal progress, recognized fibres are prohibited for further processing in the width of 7 pixels. Tracing finishes when brightness in the last pixel found does not reach a selected limit. By a special algorithm, joints of fibres are supplemented. Very small objects of skeleton are

a

b
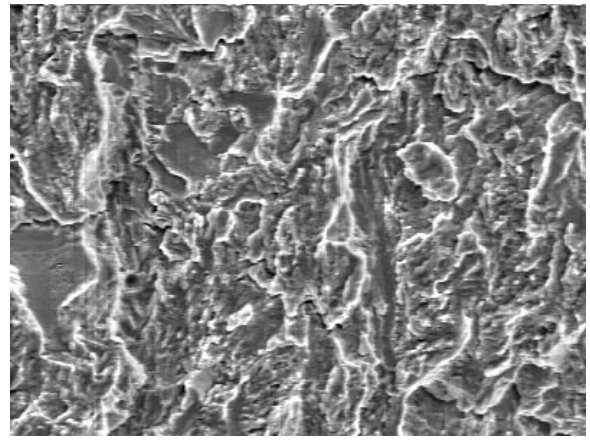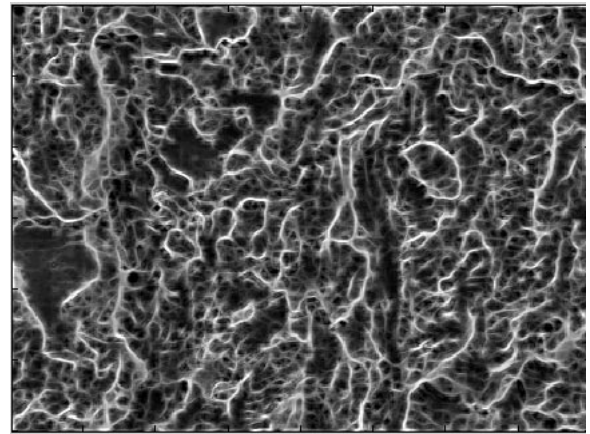
c   20 μm

Fig. 6: Extraction of light fibres from an image of fatigue crack surface.
a) normalized image (detail 400 x 300 pixels),
b) fibre detection (rescaled into 8-bit brightness scale),
c) traced significant fibres.

excluded, as they represent small non-fibrous patches.

ANALYSIS OF A FIBRE PROCESS AND CREATING A DATABASE [13]. For any description of a fibre process, the binarized image must be analyzed into elements. Three types of them are recognized: individual fibres, vertices and objects. Vertices are endpoints of fibres. Two types of vertices can be distinguished: isolated fibre endpoints, and knots - common endpoints of several fibres. An object is a continuous set of fibres.

Recognition of objects is a separate problem which can be solved by using generally recommended algorithms.

In order to classify pixels of the process as internal points, knots or vertices, the number of background-fibre changes along a curve surrounding every pixel in a given distance can be used, as it is shown in Fig.7. Simultaneously, the number of fibres leaving every vertex is obtained. The set of vertices is to be renumbered by their pertinence to objects.
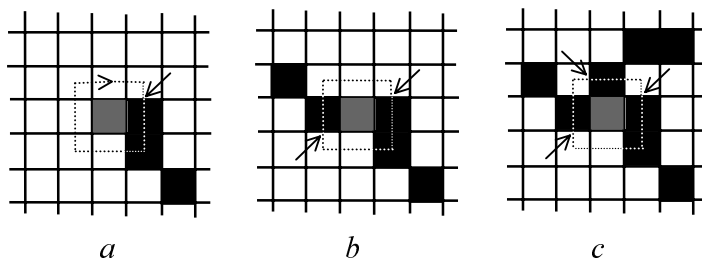

a	b	c

Fig. 7: Testing the type of pixels of the process by the number of changes backgroud - fibre along a curve surrounding the pixel. a) n = 1, endpoint, b) n = 2, internal fibre point, c) n > 2, knot.
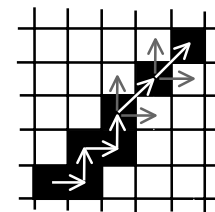
Fig. 8: Tracing a fibre with preference in row and column direction

The following step of the analysis consists in recording fibres from the starting to the finishing vertex. The simplest way is to check the neighbourhood of the size 3x3 of the last recognized pixel, while all pixels of the process recognized up to now are prohibited to avoid reversal steps. At first, row and column directions must be checked, and if no pixel has been found, also diagonal directions (Fig.8).

During the analysis, the components of the database are gradually fulfilled. The structure of the database was proposed so that it offers extracting information on objects and long fibre branches without browsing. The database can be implemented in ordinary programming languages. For computing characteristics of a higher order (e.g. mutual relations of fibres), the database should be exported to a special platform, for example MS Access, where elements of a given set of properties can be quickly selected. Although the database contains a complete description of the process and its structure, the compression in comparison to a bitmap is 80 % and higher.

Within every fibre, starting and finishing vertices are distinguished. Vertices are organized by objects and fibres by their starting vertices. So also the sequence of fibres is organized by objects.

Let n_o, n_v, n_f and n_p be numbers of objects, vertices, fibres and all pixels of the process, respectively. The database consists of four matrices:

O - the matrix of objects, size [n_o, 1].
    $O(i)$ is the number of the first vertex of object i.
V - the matrix of vertices, size [n_v, 5].
    $V(j, 1)$ is the number of the object containing vertex j,
    $V(j, 2)$ is the row coordinate of vertex j,

$V(j,3)$ is the column coordinate of vertex j,

$V(j,4)$ is the number of the first fibre starting in vertex j,

$V(j,5)$ is the position of the first fibre finishing in vertex j, in the list $F(.,4)$.

$\boldsymbol{F}$ - the matrix of fibres, size $[n_f, 4]$.

$F(k,1)$ is the number of the starting vertex of fibre k,

$F(k,2)$ is the number of the finishing vertex of fibre k,

$F(k,3)$ is the position of the first internal pixel of fibre k in the list $\boldsymbol{P}$,

$F(.,4)$ is the list of numbers of fibres ordered by the finishing vertex.

$\boldsymbol{P}$ - the matrix of internal pixels of fibres, size $[n_p\text{-}n_v, 2]$.

$P(l,1)$ is the row coordinate of pixel l,

$P(l,2)$ is the colunm coordinate of pixel l.

PARAMETRIC MODEL AND JOINING FIBRES INTO BRANCHES [13]. Let $[x_t, y_t]$, $t = 1,2,\ldots,n$ be the coordinates of the pixels of a fibre in the sequence from the starting to the finishing vertex. A moving parametric regression can be used with the length of a single regression T and the step of moving about $T/3$ (only the central third of the regression is accepted). For the regression function, we used a combination of the polynomial and poly-harmonic models (corresponding to Taylor and Fourier decomposition) in the elementary form

$$\bar{x}(t) = a_{0j} + a_{1j}\tau + a_{2j}\sin(\varphi) + a_{3j}\sin(2\varphi) \ ,$$
$$\bar{y}(t) = b_{0j} + b_{1j}\tau + b_{2j}\sin(\varphi) + b_{3j}\sin(2\varphi) \ , \tag{14}$$
$$\text{where} \quad \tau = t - t_{0j} + 1, \quad \varphi = \pi\tau / T \ .$$

Here j denotes the present recurrence of the regression and t_{0j} is its starting index. The linear component of functions (14) expresses the position and main course of the j-th segment, while the goniometric components express its "waving". A single regression does not have more than one inflection. In consequence, the maximum density of inflections of the regression is one to $T/3$ pixels of the fibre. This ratio defines the smoothing of details, which can be selected by setting T with respect to the aims of the analysis.

In every knot, all possible pairs of fibres are checked whether they create a passing branch. A common regression of merged fibres is estimated and its curvature in the knot serves for the decision. If it is smaller than a selected threshold, fibres are judged as creating a passing branch. This information is implemented in the database as 2 columns added to matrix F, where, for fibre k,

$F(k,5)$ is the number of the fibre connected in the starting vertex,

$F(k,6)$ is the number of the fibre connected in the finishing vertex.

The absence of any connection is expressed by zero.

Final regressions are computed in the same manner as described above, for joined fibres. Computing is so quick that it is not efficient to store regressions in database structures.

ESTIMATING CHARACTERISTICS OF THE FIBRE PROCESS [13]. The parametric model of a fibre process makes it possible to estimate a wide class of qualities. Characteristics of the length, direction, position and shape of branches can be computed directly and exactly, without any problems with the discrete image representation. For many cases, a sufficient source for estimating characteristics are points of regressions $[\bar{x}, \bar{y}]$ (14), that are pertinent to single pixels of binary skeletons of fibres. Increments between them can be used to estimate distributions of lengths and orientations:

$$\Delta l_{t \to t+1} = \sqrt{\left(\bar{x}(t+1) - \bar{x}(t) \right)^2 + \left(\bar{y}(t+1) - \bar{y}(t) \right)^2} \quad , \quad \phi_{t \to t+1} = arctg\left(\frac{\bar{y}(t+1) - \bar{y}(t)}{\bar{x}(t+1) - \bar{x}(t)} \right) \quad . \quad (15)$$

Also more complicated qualities can be studied - for example the joint distribution of lengths and orientations (Fig.9), the random process of the fibre orientation along its length, etc. Many of these characteristics would not be available by traditional methods.

APPLICATION [12]. For characteristics of a texture, the joint distribution of fibre length and orientation (Fig.9) was used. The sorting was roughened into four classes for the direction ($\theta \in$(-10÷10°), (-40÷-10°)$\cup$⟨10÷40°), (-70÷-40°)$\cup$⟨40÷70°), (-90÷-70°)$\cup$⟨70÷90°)) and six classes for the length (defined by class borders 10-30-50-70-100-140-500 pixels). From resulting 24 image parameters, 18 have been found to be significant in the multilinear regression at the level of significance $\alpha = 0.05$. Results are documented in Fig.10. One point represents one image. The relation of the crack length vs. the number of cycles is not visibly different from that in Fig.4.
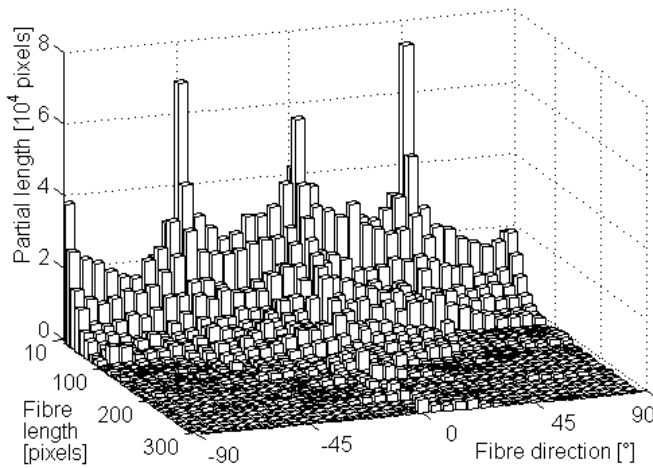

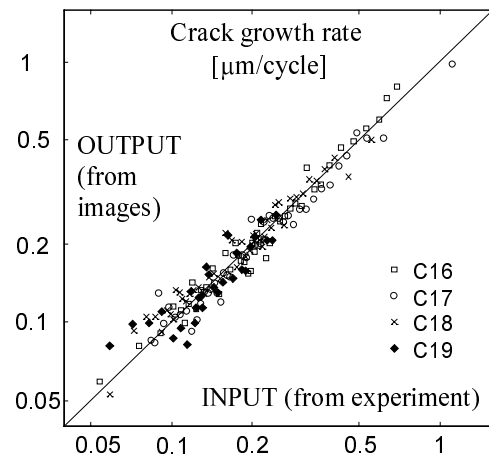Fig. 9: An example of joint distribution of the lenghts and orientations of light fibres from one image.

Fig. 10: Comparison of crack rates taken for input and given back from the fibre distribution. Ideal agreement: $y = x$.

5. CONCLUSIONS

SEM images of fatigue crack surfaces under magnifications between macro- and micro-fractography (about 30÷500 x) contain a complex image texture, which is a rich source of the information on the crack growth process. Three ways of the fractographic textural analysis have been developed to practical applicability, including routine computational programs: the spectral analysis, the modelling texture as a Gibbs random field, and the analysis of light fibres. Within all the methods, the velocity of crack growth can be estimated as a multilinear function of a set of numerical characteristics of images of fracture surfaces.

The textural fractography can complement or substitute traditional methods. It opens possibilities to obtain new information from fracture surfaces, which had been lost up now. Simultaneously, textural method transfers the main work from the operator to the computer.

Two new methods within general frame of image analysis have been developed:
- The method of tracing fibres is a practical alternative to creating a skeleton for fibre structures without distinct borders in gray scale images.

- The method of composing of a database and a parametric model of a fibre process was proposed to meet special requirements in fractography. However, the supposed character of the fibre process is general at all. The method has been fully automated and we hope that it could find a wide use in the analysis of planar fibre processes, tesselations, etc.

Acknowledgement

References

1. Pratt, W.K.: Digital image processing. John Wiley & Sons, New York 1978, pp. 235-242.
2. Parker, J.R.: Algorithms for image processing and computer vision. John Wiley & Sons, New York 1996, pp.19-23.
3. Nedbal, I. et al.: One lecture on fractography of fatigue failures. École d'Été - Dévelopments Récents en Fatigue des Matériaux et des Structures. Saint-Pierre d'Oléron, Juin 1997. École Centrale Paris - ICTM, Châtenay Malabry 1997, pp. 1-25.
4. Gimel'farb, G.L.: Image textures and Gibbs random fields. Kluwer Academic Publishers, Dordrecht 1999, 250 p.
5. Čejka, V., Beneš, V.: Computer Aided Fractography: Methods for evaluation of image anisotropy. In: Int. Conf. on Stereology, Spatial Statistics and Stochastic Geometry. Union of Czech Mathematicians and Physicists, Prague 1999, pp.89-94. ISBN 80-7015-684-8.
6. Lauschmann, H.: Computer aided fractography: The spectral analysis of fatigue crack images. In: Int. Conf. on Stereology, Spatial Statistics and Stoch. Geometry. Union of Czech Mathematicians and Physicists, Prague 1999, pp.171-176. ISBN 80-7015-684-8.
7. Lauschmann, H.: Textural analysis of fatigue crack surfaces - Image pre-processing. Acta Polytechnica Vol.40 No.4, CTU Prague 2000, pp.123-129, ISBN 80-01-02055-X.
8. Lauschmann, H., Adámek, J., Nedbal, I.: Textural fractography: Sectral analysis of images of fatigue crack surfaces. In: Fractography 2000. Ed. L. Parilák. Institute of Materials Research of the Slovak Academy of Sciences, Košice 2000, pp.313-320. ISBN 80-968468-3-3.
9. Nedbal, I., Kunz, J., Siegl, J.: Influence of corrosion environment and stress ratio on fatigue crack growth in stainless steel 304 L. In: Fractography 2000. Ed. L. Parilák. : Institute of Materials Research of the Slovak Academy of Sciences, Košice 2000, pp. 293-300. ISBN 80-968468-3-3.
10. Lauschmann, H., Wetzig, K., Menzel, S., Göbel, T.: Fractography of crack networks in thin layers. Materials Characterization 46 (2001), pp. 105-111.
11. Lauschmann, H., Ráèek, O.: Textural fractography: Application of Gibbs random fields. In: Proc. 3rd Int. Conf. Materials Structure & Micromechanics of Fracture, Brno June 27-29, 2001. Brno University of Technology, 2001.
12. Lauschmann, H., Tůma, M., Ráèek, O., Nedbal, I.: Textural fractography. 8th European Congress for Stereology & Image Analysis, Bordeaux Sept. 3-7, 2001. Image Analysis and Stereology, 2001, 20 (Suppl.1), pp. 372-378. ISBN 961-90933-0-5 (ISSN 1580-3139).
13. Lauschmann, H.: A database-oriented analysis of a fibre process in fractography. 8th European Congress for Stereology & Image Analysis, Bordeaux Sept. 3-7, 2001. Image Analysis and Stereology, 2001, 20 (Suppl.1), pp. 379-385. ISBN 961-90933-0-5 (ISSN 1580-3139).